

Topology of the yeast fatty acid transport protein Fat1p: mechanistic implications for functional domains on the cytosolic surface of the plasma membrane

Thomas Obermeyer,^{*,†} Peter Fraisl,^{*} Concetta C. DiRusso,^{*,†} and Paul N. Black^{1,*,†}

Center for Metabolic Disease, Ordway Research Institute,^{*} and Center for Cardiovascular Sciences,[†] Albany Medical College, Albany, NY 12208

Abstract The fatty acid transport protein (FATP) Fat1p in the yeast *Saccharomyces cerevisiae* functions in concert with acyl-coenzyme A synthetase (ACSL; either Faa1p or Faa4p) in vectorial acylation, which couples the transport of exogenous fatty acids with activation to CoA thioesters. To further define the role of Fat1p in the transport of exogenous fatty acids, the topological orientation of two highly conserved motifs [ATP/AMP and FATP/very long chain acyl CoA synthetase (VLACS)], the carboxyl 124 amino acid residues, which bind the ACSL Faa1p, and the amino and carboxyl termini within the plasma membrane were defined. T7 or hemagglutinin epitope tags were engineered at both amino and carboxyl termini, as well as at multiple non-conserved, predicted random coil segments within the protein. Six different epitope-tagged chimeras of Fat1p were generated and expressed in yeast; the sidedness of the tags was tested using indirect immunofluorescence and protease protection by Western blotting. Plasma membrane localization of the tagged proteins was assessed by immunofluorescence. Fat1p appears to have at least two transmembrane domains resulting in a N_{in}-C_{in} topology. We propose that Fat1p has a third region, which binds to the membrane and separates the highly conserved residues comprising the two halves of the ATP/AMP motif. The N_{in}-C_{in} topology results in the placement of the ATP/AMP and FATP/VLACS domains of Fat1p on the inner face of the plasma membrane. The carboxyl-terminal region of Fat1p, which interacts with ACSL, is likewise positioned on the inner face of the plasma membrane. This topological orientation is consistent with the mechanistic roles of both Fat1p and Faa1p or Faa4p in the coupled transport/activation of exogenous fatty acids by vectorial acylation.—Obermeyer, T., P. Fraisl, C. C. DiRusso, and P. N. Black. **Topology of the yeast fatty acid transport protein Fat1p: mechanistic implications for functional domains on the cytosolic surface of the plasma membrane.** *J. Lipid Res.* 2007. 48: 2354–2364.

Supplementary key words fatty acid transport protein • topology • functional domains

Manuscript received 31 August 2006 and in revised form 29 June 2007.

Published, JLR Papers in Press, August 6, 2007.

DOI 10.1194/jlr.M700300-JLR200

Unlike sugars, amino acids, and nucleotides, fatty acids are very apolar compounds and readily partition into biological membranes (1–5). The free fatty acid concentrations in the circulation, in the extracellular milieu, and within cells are quite low as a consequence of their relative insolubility under aqueous conditions. To compensate for this low solubility, most organisms have evolved specific mechanisms to transport fatty acids, including lipid binding proteins such as serum albumin and fatty acid binding protein, or to store fatty acids esterified in complex lipids. The complex lipids are trafficked in lipoprotein particles and sequestered within membranes or lipid bodies. The mechanisms governing fatty acid transport across the plasma membrane are distinct from other classically defined transport processes and involve both diffusional and protein-mediated components. Current evidence has demonstrated that fatty acid translocase/CD36 (FAT/CD36), fatty acid transport protein (FATP), and long-chain acyl-coenzyme A synthetase (ACSL) function in the trafficking of exogenous long-chain fatty acids across the plasma membrane (1, 3, 5). The mechanistic details of how FAT/CD36 and FATP function in this process are elusive, but both transgenic and knockout models indicate that these proteins provide important determinants in the transmembrane movement of exogenous long-chain fatty acids (6–14). Despite this information, the precise role of these proteins in the trafficking of fatty acids is clouded in that both have other biochemical activities. FAT/CD36, for example is a member of a broad family of scavenger receptors and acts as a receptor for thrombospondin, collagen, oxidized low density lipoprotein, and anionic phospholipids, in addition to fatty acids (1). Members of the FATP family have also been described as very long-chain ACSLs, suggesting that they, like ACSL, may function in transport by activating exogenous fatty acids (13–20).

Abbreviations: VLACS, very long chain acyl CoA synthetase.

¹To whom correspondence should be addressed.

e-mail: pblack@ordwayresearch.org

Copyright ©2007 by the American Society for Biochemistry and Molecular Biology, Inc.

Our work, using the yeast *Saccharomyces cerevisiae* as a model, provides a platform to establish the mechanistic framework of how FATP and ACSL function in the trafficking of exogenous long-chain fatty acids across the plasma membrane (2, 16, 21–27). In yeast, both a FATP and a cognate ACSL are required for this process (24, 25). Our previous work using directed mutagenesis of the yeast FATP ortholog Fat1p showed that functional elements contributing to very long-chain fatty acid activation and long-chain fatty acid transport are distinguishable (26). Subsequent work demonstrated that Fat1p and ACSL (Faa1p or Faa4p) form a complex, which functions to promote the transmembrane movement-coupled activation of fatty acids via a process called vectorial acylation (27). Yeast two-hybrid and negative dominant studies have specifically shown that the carboxyl end of Fat1p interacts with Faa1p (27). Further multicopy suppression studies have shown that when overexpressed, Fat1p has detectable levels of oleoyl-CoA synthetase activity (27). More recently, our laboratory has shown that three murine isoforms of FATP (1, 2, and 4) are fully functional in the transport of exogenous long-chain fatty acids when expressed in yeast and complement the growth and biochemical phenotypes associated with a deletion in *FAT1* (23). These data suggest that at least these three FATP isoforms function as components of a fatty acid transport system localized to the plasma membrane, which is linked to downstream fatty acid trafficking.

Mechanistic attributes and correlating predicted structural features intrinsic to the different FATP members remain largely unknown. Members of this family contain two functional domains, which are highly conserved (2). The ATP/AMP binding motif is common to all adenylate-forming enzymes, and the FATP/very long chain acyl CoA synthetase (VLACS) motif is conserved among the FATP family of proteins and divergent compared with the ACSL members. Data arising from our directed mutagenesis studies are consistent with the notion that the FATP/VLACS motif contributes to functional elements within the protein directly involved in fatty acid transport (26). Interestingly, the region of Fat1p that exerts a negative dominant effect and interacts with the ACSL Faa1p is just downstream from this motif (27). These findings are consistent with the conclusion that Fat1p functions in concert with Faa1p in the coupled transport and activation of exogenous fatty acids before downstream trafficking. In support of the concept of vectorial acylation requiring a FATP and a cognate ACSL, studies by Richards et al. (28) have shown that murine FATP1 and ACSL1 also form a functional complex in the plasma membrane of adipocytes.

To establish the function of Fat1p in the trafficking of exogenous long-chain fatty acids across the plasma membrane, the current study was directed at defining the topology of this protein within the plasma membrane. Of particular importance was to establish the topological placement of the ATP/AMP and FATP/VLACS motifs relative to the amino and carboxyl termini of the protein. T7 and hemagglutinin (HA) epitope tags were engineered into different regions of Fat1p, and topological placement was determined using a combination of indirect immuno-

fluorescence and protease protection coupled with Western blotting. This work supports a $N_{in}-C_{in}$ membrane topology of Fat1p, resulting in two transmembrane helices and the topological positioning of the highly conserved domains adjacent to the membrane on the interior of the cell.

EXPERIMENTAL PROCEDURES

Strains, media, and materials

The *S. cerevisiae* strain LS2086 (*faa1Δ1.9::HIS3 fat1Δ0.48::G418*) used in this study has been described previously (27); the plasmids used in this study are described below. Yeast strains were routinely transformed using lithium acetate (29). Yeast-supplemented minimal medium contained 0.67% yeast nitrogen base (YNB), 2% dextrose, adenine (20 mg/l), uracil (20 mg/l), and amino acids as required. To induce protein expression, cells were grown in YNB containing 2% galactose and 2% raffinose (YNBGR). Growth in YNBGR medium was monitored by optical density at 600 nm; for all experiments, cells were mid-log phase at 30°C (1×10^7 cells/ml). For complementation studies, cells were grown at 30°C on YNBGR agar plates supplemented with 45 μM cerulenin and 100 μM oleate.

Plasmids were maintained in the *Escherichia coli* strain C600. Growth of bacterial cultures was monitored using a Klett-Summerson colorimeter equipped with a blue filter. Plasmids were purified using Qiagen kits and were sequenced to confirm the placement of the different T7 and HA epitopes.

Yeast extract, yeast peptone, and YNB were obtained from Difco. Oleic acid was obtained from Sigma. Zymolyase 20T (*Arthrobacter luteus*) was purchased from ICN Biochemicals. 4,4-Difluoro-5-methyl-4-bora-3a,4a-diaza-s-indacene-3-dodecanoic acid (C₁-BODIPY-C₁₂) was purchased from Molecular Probes. Enzymes required for all DNA manipulations were from Promega, Invitrogen, or New England Biolabs. PCR primers were purchased from Integrated DNA Technologies. Mouse anti-T7 and rabbit anti-HA were purchased from Invitrogen and Sigma, respectively; Alexa Fluor 488 goat anti-rabbit IgG, Alexa Fluor 594 donkey anti-mouse IgG, and mouse anti-Vma2p were from Molecular Probes; and HRP goat anti-mouse IgG and HRP goat anti-rabbit IgG were from Promega. Anti-Pma1p was a gift from Dr. Guenther Daum; anti-Gas1p and anti-Sec61p were gifts from Drs. Howard Reizman and Randy Schekman, respectively.

Algorithms to predict transmembrane topology

Three algorithms were used to predict the transmembrane topology of Fat1p. The first, a hydrophobicity plot, was based on the hydrophobic properties of individual amino acid residues using an average length of nine amino acid residues (30). The second, TMPred (31), predicts both transmembrane-spanning regions and orientation using statistical analyses of a database of known transmembrane proteins (http://www.ch.embnet.org/software/TMPRED_form.html). The third, MEMSTAT3 (32), also predicts transmembrane segments and orientation using the protein structure prediction server (<http://bioinf.cs.ucl.ac.uk/psipred/psiform.html>). The sequence of Fat1p was submitted to SWISS-MODEL [<http://swissmodel.expasy.org/>] (33) using the structures of the adenylate-forming enzymes firefly luciferase [Protein Data Bank (PDB) number 1LCI (34)], yeast acetyl-CoA synthetase [PDB 1RY2 (35)], and *Thermus thermophilus* ACSL [PDB 1V26 (36)] as templates and using the first approach mode to determine whether a structure of this protein could be predicted. In all cases, the alignments lacked sufficient identity to permit modeling.

Construction of expression plasmids encoding epitope-tagged versions of Fat1p

The yeast expression vector pDB121 and the ¹⁷Fat1p expression plasmid pDB304 have been described previously (26). The different Fat1p epitope chimeras were generated using overlap extension PCR using pDB304 as the template. Five sites were chosen for insertion of the HA epitope (YPYDVPDYA) within Fat1p: Q⁸⁸-HA-N⁸⁹, designated Fat1p^{Q88-HA}, was located between two predicted amino-terminal proximal α helices; D¹⁹³-HA-A¹⁹⁴, designated Fat1p^{D193-HA}, was located between the second predicted transmembrane helix and the conserved ATP-AMP motif; N⁵⁷⁹-HA-S⁵⁸⁰ and Y⁶⁴⁸-HA-K⁶⁴⁹, designated Fat1p^{N579-HA} and Fat1p^{Y648-HA}, respectively, were located in the carboxyl portion of the protein; and at the carboxyl end of Fat1p, which was designated Fat1p^{HA}. Table 1 lists the oligonucleotides used to generate each of the epitope-tagged Fat1p constructs. These sites were selected as random coil and antigenic segments of the protein, computed with the PROTEAN algorithm in the LaserGene software (DNASStar). All PCRs were carried out according to cycling and reagent conditions specified by the manufacturer. The completed plasmid constructs were sequenced to verify the placement of the epitope and to ensure that no other mutations were generated in the PCRs.

Expression and localization of epitope-tagged derivatives of Fat1p

Cells (*faa1 Δ fat1 Δ*) transformed with pDB121, pN304, or the Fat1p epitope derivatives were grown under inducing conditions in YNBGR (with appropriate supplements) to mid-log phase (absorbance at 600 nm = 0.8–1.0) for all experiments. For the localization studies, cells were harvested by centrifugation after growth to mid-log phase, washed twice with PBS, and resuspended to a density of 5.0×10^8 cells/ml in 10 ml of 10 mM Tris, pH 7.5, 0.2 mM EDTA, 0.2 mM dithiothreitol, and 25 μ M PMSF. The resuspended cells were lysed using glass beads by vigorous vortexing on ice for 10 min; total membrane and plasma membranes were isolated as detailed by Zinser and Daum (37). For the plasma membranes, two discontinuous sucrose gradients were routinely used. The expression of the Fat1p and epitope-tagged derivatives in total cell lysates, total membrane, and purified plasma membranes were monitored using Western blots probed with anti-T7 antibody. Anti-Gas1p and anti-Sec61p were used as plasma membrane and endoplasmic reticulum markers, respectively.

Determination of very long-chain ACSL activity

Very long-chain ACSL activity in cell extracts expressing ¹⁷Fat1p or the epitope-tagged derivatives of Fat1p was measured

using standard conditions as described previously (26). The standard reaction mixtures contained 50 mM Tris-HCl, pH 8.0, 10 mM ATP, 10 mM MgCl₂, 0.3 mM DTT, 0.001% Triton X-100, 50 μ M [¹⁴C]lignocerate (from a 10 \times stock prepared in 10 mg/ml α -cyclodextrin), and 200 μ M CoA. Fatty acid stocks were prepared as free acids. The reaction was initiated by the addition of CoA at 30°C, continued for 15 min, and terminated by the addition of 2.5 ml of isopropanol- η -heptane-1 M H₂SO₄ (40:10:1). The free fatty acid was removed by sequential organic extractions using η -heptane. Very long-chain acyl-CoA formed during the reaction remained in the aqueous fraction and was quantified by scintillation counting.

Fatty acid transport monitored using the fluorescent fatty acid C₁-BODIPY-C₁₂

After growth under inducing conditions, cells were harvested and resuspended in 0.5 ml of PBS (6×10^7 cells/ml). All steps were performed at room temperature. Accumulation of C₁-BODIPY-C₁₂ as an indicator of fatty acid transport capacity was monitored using confocal laser-scanning microscopy (38). Cells were incubated with 5 μ M C₁-BODIPY-C₁₂ for 3 min, washed three times with PBS containing 15 μ M fatty acid-free BSA, resuspended in PBS, placed on a poly-L-lysine-treated multiwell slide (ICN Fisher Scientific, Pittsburgh, PA), and visualized using confocal laser-scanning microscopy. The instrument settings for brightness and contrast were optimized to ensure that the confocal laser-scanning microscope was set for full dynamic range relative to cells without Fat1p (*faa1 Δ fat1 Δ* cells transformed with the vector pDB121) and those expressing yeast Fat1p [*faa1 Δ fat1 Δ* cells transformed with pDB304 (encoding ¹⁷Fat1p)]. The same settings were used for all subsequent image collections. An argon laser source was used for imaging, with excitation at 488 nm and emission at 505 nm.

Immunofluorescence

Cells (*faa1 Δ fat1 Δ*) transformed with pDB121 (vector), pDB304 (encoding ¹⁷Fat1p), or the epitope-tagged derivatives of pDB304 were grown under inducing conditions as detailed above. Cells were grown to mid-log phase, formaldehyde was added to a final concentration of 2%, and incubation was continued at room temperature with gentle shaking for 10 min (39). The fixed cells were harvested by centrifugation at 4,000 g, resuspended in PBS containing 3.7% formaldehyde, shaken for 90 min at room temperature, rinsed twice with PBS, resuspended to a density of $\sim 5 \times 10^8$ cells/ml in spheroplasting buffer (PBS, 1.2 M sorbitol, 25 mM 2-mercaptoethanol, and 350 μ g/ml Zymolyase 20T), and incubated at 37°C for 30 min. The resultant spheroplasts were

TABLE 1. PCR primers used to generate the Fat1p epitope-tagged constructs in this study

Fat1p ^{Q88-HA}	Reverse, 5'- <u>AGC GTA ATC TGG AAC ATC GTA TGG GTA</u> TTG TTG GAC CTG TTT AAT AAA-3'
	Forward, 5'-TAC CCA TAC GAT GTT CCA GAT TAC GCT AAT GGT GAC CAT TTA GCG ATT-3'
Fat1p ^{N193-HA}	Reverse, 5'-AGC GTA ATC TGG AAC ATC GTA TGG GTA ATC AGG GTC AAT AAA TAC CTG-3'
	Forward, 5'-TAC CCA TAC GAT GTT CCA GAT TAC GCT GCC AGT AAT CCG ATC AGA GAA-3'
Fat1p ^{N579-HA}	Reverse, 5'-AGC GTA ATC TGG AAC ATC GTA TGG GTA GTT GTC AGT TAG TTT AAT AAC-3'
	Forward, 5'-TAC CCA TAC GAT GTT CCA GAT TAC GCT TCT CTT GAC ATC ACT GCA AAG-3'
Fat1p ^{Y648-HA}	Reverse, 5'-AGC GTA ATC TGG AAC ATC GTA TGG GTA GTA ATT CTT GAG CCA AAA AAT-3'
	Forward, 5'-TAC CCA TAC GAT GTT CCA GAT TAC GCT AAG CGC TAT GAA GTC TTG ACC-3'
Fat1p ^{HA}	Reverse, 5'-AGC GTA ATC TGG AAC ATC GTA TGG GTA TAA TTT AAT TGT TTG TGC ATC-3'
	Forward, 5'-TAC CCA TAC GAT GTT CCA GAT TAC GCT TGA TTT GAT GTT CCT GAA TTA-3'

HA, hemagglutinin. The underlined sequences encode the HA tag.

gently pelleted using centrifugation (3,000 g, 10 min), washed once, and then resuspended in sorbitol buffer (PBS, 1.2 M sorbitol, and 25 mM 2-mercaptoethanol). Each sample of spheroplasts was split into two samples; the first was fixed-only, and the second was permeabilized (fixed-permeabilized) by the addition of Triton X-100 to 0.2%. The resuspended spheroplasts (fixed-only or fixed-permeabilized) were dropped into wells of a multiwell slide (ICN Fisher Scientific) that had been pre-cleaned and coated with 0.1% poly-L-lysine. The slides were placed in a humidified chamber for 10 min to allow the spheroplasts to settle and adhere. All antibody staining was carried out either in PBS plus 1 mg/ml BSA for fixed-only spheroplasts or in the same solution plus 0.1% Tween 20 for fixed-permeabilized spheroplasts. The primary antibodies were added, and samples were incubated in a humidified chamber for 1 h at room temperature. The wells were washed three times with the sorbitol buffer and then incubated for 1 h with the appropriate fluorescence-conjugated secondary antibody. The wells were again washed, filled with mounting medium (1 mg/ml *p*-phenylenediamine in 80% glycerol/20% PBS), and sealed under a coverslip. Slides were examined and photographed using a Zeiss LSM510 Meta confocal microscope (Carl Zeiss MicroImaging, Inc., Thornwood, NY). An argon laser source was used for imaging; for Alexa Fluor 488 and Alexa Fluor 594 conjugates, excitation/emission conditions were 495/519 nm and 590/617 nm, respectively. Images were exported to Photoshop CS2 (version 7.0; Adobe), grouped, and adjusted for brightness, color balance, and contrast.

Protease protection and Western blotting

Spheroplasts were prepared from the *faa1Δfat1Δ* yeast cells as detailed above but without the initial fixation step using formaldehyde. The final preparations of spheroplasts were resuspended in 100 mM potassium phosphate, pH 7.5, containing 1.2 M sorbitol and, as above, split into two samples. Triton X-100 was added to one sample to a final concentration of 0.2%. Spheroplasts (intact or permeabilized; ~20 μg of total protein) were treated with varying concentrations of trypsin at 30°C for 15 min. The reactions were terminated by the addition of PMSF at a final concentration of 10 mM and washing once with 100 mM potassium phosphate, pH 7.5, and 1.2 M sorbitol. The spheroplasts were immediately solubilized with 200 mM NaOH and 2% 2-mercaptoethanol, and total protein was precipitated with 5% TCA. Protein samples were prepared, separated by SDS-PAGE, and transferred to a nitrocellulose membrane. The Western blots were developed using the primary antibodies noted above, HRP-conjugated secondary goat-anti rabbit or goat anti-mouse antibodies, and developed using enhanced chemiluminescence (Amersham).

RESULTS

Bioinformatics prediction of Fat1p topology and relationships to functional domains

The membrane topology of Fat1p was predicted using three different algorithms: Kyte and Doolittle (30), TMpred (31), and MEMSTAT3 (32) (Fig. 1). The Kyte and Doolittle and TMpred algorithms predicted that regions A and B were of sufficient length to traverse the membrane once, whereas region C could possibly traverse the membrane twice. The regions of Fat1p, which contains the highly conserved ATP/AMP motif common to all adenylate-forming enzymes, are found between residues 256 and 271 and 339

and 356. The hydrophobic area of Fat1p noted as region C is between the two halves of the ATP/AMP motif. The FATP/VLACS motif, which is important for both fatty acid transport and very long-chain ACSL activity, is between residues 491 and 540 and in a region of the protein that is more hydrophilic; the negative dominant peptide, which functions to depress long-chain ACSL activity of the ACSL Faa1p, is just downstream from the FATP/VLACS motif and likewise more hydrophilic.

TMpredict (Fig. 1B) suggested two models for the transmembrane topology of Fat1p. The first had the N terminus of Fat1p on the outside face of the membrane and three transmembrane helices, resulting in a $N_{out}-C_{in}$ topology; the second suggested that the N terminus of Fat1p was on the inside face and also had three transmembrane helices, resulting in a $N_{in}-C_{out}$ orientation. We suspected that both alternatives were flawed, as they would have placed the two halves of the ATP/AMP motif on opposite sides of the membrane. We next predicted the transmembrane topology of Fat1p using MEMSTAT3 (32). These analyses predicted four transmembrane domains, resulting in a $N_{in}-C_{in}$ topology. In this model, the hydrophobic region noted as C between the two halves of the ATP/AMP motif was predicted to form two helices (residues 278–306 and 308–327). In this orientation, both halves of the ATP/AMP motif would be placed on the inside surface of the membrane and likely in juxtaposition to one another. In addition, the $N_{in}-C_{in}$ transmembrane topology of Fat1p, with four transmembrane segments, placed the FATP/VLACS motif on the inside surface of the membrane, which we felt was essential given the functional properties of this region of the protein.

Gertow et al. (40) presented a model of the murine fatty acid transport protein 4 (mmFATP4) developed using 3D-PSSM (41) and related that information to a polymorphism at residue 209 that is associated with insulin resistance. Our attempts to model Fat1p using 3D-PSSM were unsuccessful, in part because the template folds used to predict structure have not been updated since 2003. Rather, we addressed whether a predicted structure of Fat1p could be generated with SWISS-MODEL (33) using the structures of three known adenylate-forming enzymes as templates (see Experimental Procedures), as we had previously done for the bacterial long-chain ACSL (42). These efforts to model a predicted structure of Fat1p were also unsuccessful, because the alignments of Fat1p to all three adenylate-forming enzymes were of insufficient quality.

Construction and expression of epitope-tagged derivatives of Fat1p

The transmembrane topology of Fat1p predicted using the algorithms discussed above offered several alternatives, with the last ($N_{in}-C_{in}$) being the most convincing given the function of this protein. In the absence of structural data for Fat1p, we chose to test the predicted transmembrane topology using a series of epitope-tagged derivatives. Fat1p constructs were generated with either a T7 tag at the N terminus or an HA tag at various locations within the protein (Fig. 1C). The positions within Fat1p chosen

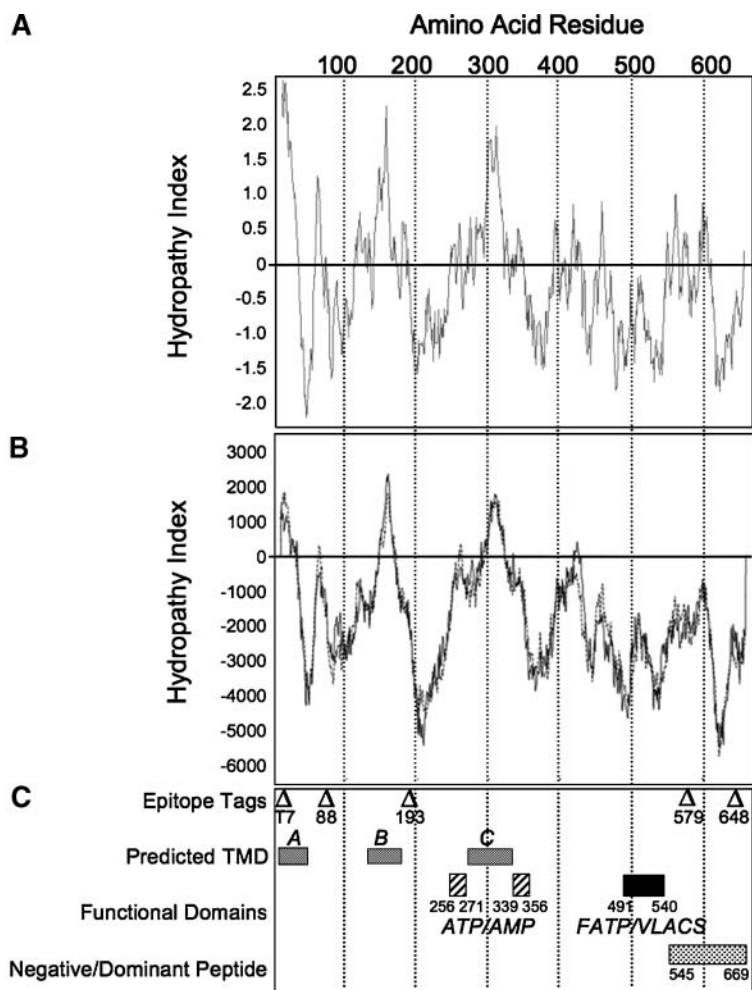


Fig. 1. Algorithms used to predict the transmembrane topology of Fat1p. A: The Kyte-Doolittle hydrophobicity plot for Fat1p using an average length of nine amino acid residues (30). B: The hydropathy plot for Fat1p generated using TMpred (31). C: The positions of the different epitope-tagged forms of Fat1p are indicated with open triangles. The algorithm MEMSTAT3 (32) was used to define the predicted transmembrane domains (TMD), denoted A, B, and C above the corresponding rectangles. The regions of Fat1p corresponding to the ATP/AMP and fatty acid transport protein (FATP)/very long chain acyl CoA synthetase motifs are shown as functional domains. The position of the negative dominant peptide is noted by the light gray rectangle (27).

for the introduction of the epitope tags were based upon their predicted antigenicity and random coil folding pattern and were at locations outside of the algorithm-predicted transmembrane helices. Our rationale was to avoid regions of the protein critical for structural integrity. Additionally, regions within the protein that were predicted to be functional domains based on similarities to other FATP proteins (the ATP/AMP motif, common to all adenylate-forming enzymes, and the FATP/VLACS motif, common to FATP family members) were not included so as to preserve protein function. Four sites within Fat1p were chosen for the introduction of HA epitope tags: Q⁸⁸-N⁸⁹, D¹⁹³-A¹⁹⁴, N⁵⁷⁹-S⁵⁸⁰, and Y⁶⁴⁸-K⁶⁴⁹; these are designated Fat1p^{Q88-HA}, Fat1p^{D193-HA}, Fat1p^{N579-HA}, and Fat1p^{Y648-HA}, respectively. Each of these constructs also contained an amino-terminal T7 epitope tag. Two additional constructs were generated that contained 1) an amino-terminal T7 tag (^{T7}Fat1p) or 2) both amino-terminal T7 and carboxyl-terminal HA tags (Fat1p^{HA}). DNA sequencing verified each construct and demonstrated that the open reading frames were intact.

All epitope-tagged Fat1p derivatives were expressed to comparable levels in extracts of whole yeast cells, as monitored by immunoblotting with anti-T7 antibody (Fig. 2). The HA tag within Fat1p^{Q88-HA}, Fat1p^{D193-HA}, Fat1p^{N579-HA}, and Fat1p^{Y648-HA} was likewise detectable (Fig. 2). The carboxyl-

terminal HA tag on Fat1p^{HA} was particularly reactive, even though the protein was expressed at levels comparable to all of the other constructs (data not shown). Consistent with earlier work, ^{T7}Fat1p was localized at the plasma membrane (Fig. 3); each of the epitope-tagged derivatives of Fat1p were likewise partially localized to the plasma membrane. Previous work has shown that Fat1p is also localized to intracellular sites, including the endoplasmic reticulum and lipid body (43). We initially tested the complementation of each of these epitope constructs for the ability to rescue growth on agar plates containing oleate and cerulenin. The expression of ^{T7}Fat1p, Fat1p^{Q88-HA}, Fat1p^{N579-HA}, and Fat1p^{L648-HA} was able to support growth, whereas the expression of Fat1p^{D193-HA} was not (data not shown). The fatty acid transport profiles using C₁-BODIPY-C₁₂ after the expression of the different epitope-tagged constructs mirrored the complementation data: ^{T7}Fat1p, Fat1p^{Q88-HA}, Fat1p^{N579-HA}, and Fat1p^{L648-HA} fully restored the fatty acid transport, whereas Fat1p^{D193-HA} did not (Fig. 4). The levels of uptake were quantified, which showed that each construct, with the exception of Fat1p^{D193-HA}, was functional in transport, albeit reduced compared with the wild type (Table 2).

We next addressed whether the expression of these epitope-tagged constructs of Fat1p disrupted very long-chain ACSL activity (Table 2). Like the growth and transport phenotypes only, ^{T7}Fat1p, Fat1p^{Q88-HA}, Fat1p^{N579-HA},

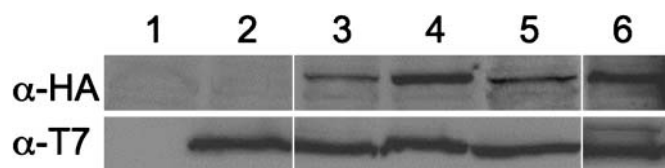


Fig. 2. Western blots showing the expression of each of the epitope-tagged derivatives of Fat1p. The upper panel was probed with anti-hemagglutinin (α -HA), and the lower panel was probed with anti-T7 (α -T7). The protein concentration for each sample was 20 μ g/lane. Lane 1, vector control (no Fat1p); lane 2, T^7 Fat1p; lane 3, Fat1p^{Q88-HA}; lane 4, Fat1p^{D193-HA}; lane 5, Fat1p^{N579-HA}; lane 6, Fat1p^{Y648-HA}. The vertical white lines indicate different films used to generate the composite figure. The blots shown are representative of seven independent experiments.

and Fat1p^{L648HA} were able to restore very long-chain ACSL activities to at least 50% of wild-type levels. Fat1p^{D193-HA} was expressed, but apparently as an inactive protein. We suspect that this epitope may result in misfolding or improper alignment of functional elements within the protein. Given that T^7 Fat1p, Fat1p^{Q88-HA}, Fat1p^{N579-HA}, and Fat1p^{L648-HA} were able to complement the fatty acid transport and very long-chain ACSL defects in the *faa1 Δ fat1 Δ* strain, we chose these constructs to assess the topology of Fat1p and test which transmembrane model was likely to be correct.

Immunofluorescence shows that the amino and carboxyl regions of Fat1p are located on the inner face of the plasma membrane

Spheroplasts were prepared from cells expressing T^7 Fat1p, Fat1p^{Q88-HA}, and Fat1p^{Y648-HA}, fixed, treated with buffer (intact) or Triton X-100 (permeabilized), and analyzed by immunofluorescence using anti-T7 and anti-HA sera. Anti-T7 and anti-HA did not recognize the amino-

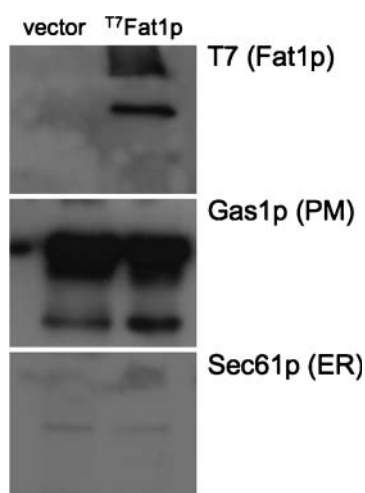


Fig. 3. Plasma membrane localization of T^7 Fat1p. Plasma membranes were purified from cells transformed with vector (vector) or a plasmid expressing T^7 Fat1p (T^7 Fat1p), and Western blots were probed for Fat1p using anti-T7 (top panel). Controls are shown for plasma membrane (PM) using anti-Gas1p antibody (middle panel) and for endoplasmic reticulum (ER) contamination using anti-Sec61 antibody (bottom panel). The blots shown are representative of three independent experiments.

and carboxyl-terminal epitope tags in T^7 Fat1p and Fat1p^{Y648-HA}, respectively, in the intact spheroplasts, supporting the conclusion that two terminal regions of Fat1p are on the intracellular side of the membrane (Fig. 5A, B). When the same spheroplasts were permeabilized with Triton X-100 after fixation, both epitope tags were recognized. The regions recognized are likely to correspond to the plasma membrane and to intracellular sites, including the endoplasmic reticulum and lipid body, consistent with earlier data (43). When the same experimental strategies were applied to cells expressing Fat1p^{Q88-HA}, the HA epitope was recognized in both intact and permeabilized cells, indicating that this epitope is exposed at the cell surface (Fig. 5A, B). As expected for a surface-exposed epitope, the polyclonal antibody against the plasma membrane-bound ATPase Pma1p identified the protein in both the intact and permeabilized spheroplasts (Fig. 5A, B).

The immunofluorescence data from T^7 Fat1p, Fat1p^{Q88-HA}, and Fat1p^{L648-HA} support the topology of Fat1p as N_{in} - C_{in} . These data are consistent with a minimum of two transmembrane helices, noted as A and B in Fig. 1. Both helices are predicted to be amino-terminal proximal. The first includes residues 18–37, and the second includes residues 146–169, as predicted using MEMSTAT3. Fat1p^{Q88-HA} resides on the outer face of the membrane between the two helices. As noted above, the third hydrophobic region of Faa1p lies between the two halves of the highly conserved ATP/AMP motif, which, using directed mutagenesis, we have shown to be crucial for Fat1p function. Within the first half of the ATP/AMP motif are Y²⁵⁶, S²⁵⁸, and T²⁶⁰, which, when substituted with an alanine, severely depress or eliminate very long-chain ACSL activity but have less of an impact on fatty acid transport. Of particular note is the S²⁵⁸ substitution to alanine, which has no very long-chain ACSL activity but still retains fatty acid transport activity at 41% of wild-type levels (26). Mutations within the second half depress very long-chain ACSL to between 17% and 32% of wild-type levels, with a commensurate reduction in fatty acid transport (26). We presume that both halves of the ATP/AMP motif reside on the intracellular face of the plasma membrane. Substitution of F³²⁵ to alanine was rather severe, particularly at the level of fatty acid transport. MEMSTAT3 predicts F³²⁵ to be on the inner face of the membrane and at the end of the second of two helices that constitute the hydrophobic region between the two halves of the ATP/AMP motif. The finding that Fat1p^{F325A} has reduced transport and activation activities is consistent with the notion that this hydrophobic region of Fat1p plays an important role by aligning the two halves of the ATP/AMP motif.

Limited proteolysis of spheroplasts using trypsin supports the N_{in} - C_{in} topology of Fat1p

Proteolytic digestion with trypsin or a similar protease has been used to assess the topology of a number of yeast and mammalian plasma membrane-bound proteins (24–26). Using this approach, only sites containing accessible protease recognition sequences are capable of being cleaved. By combining an approach using intact and

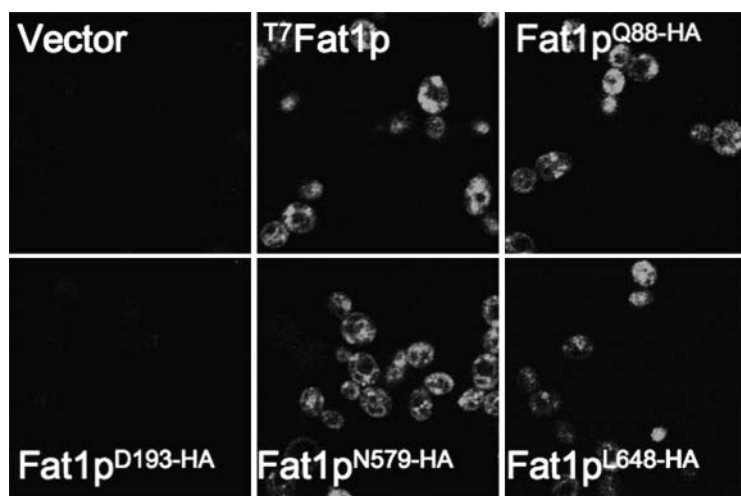


Fig. 4. Transport of 4,4-difluoro-5-methyl-4-bora-3a,4a-diaza-*s*-indacene-3-dodecanoic acid (C_1 -BODIPY- C_{12}) by selected epitope-tagged forms of Fat1p and viewed using confocal microscopy.

detergent-permeabilized cells (or spheroplasts in the case of yeast) and a protein with different epitope tags, the orientation of a given protein can be experimentally determined. The data presented above support the topology of Fat1p as N_{in} - C_{in} , with two transmembrane segments that are likely to include residues 18–37 and 146–169. In control experiments, the integrity of spheroplasts, prepared as detailed in Experimental Procedures, was assessed after trypsinolysis with the detection of the plasma membrane glycosylphosphatidylinositol-anchored protein Gas1p and the vacuolar (intracellular) protein Vma2p (Fig. 6). Within intact spheroplasts, both Gas1p and Vma2p were detected using their respective antibodies. As the concentration of trypsin increased, the levels of Gas1p decreased, as expected for a protein exposed on the outer leaflet of the plasma membrane. By comparison, Vma2p as an intracellular protein remained intact at concentrations up to 1 mg/ml trypsin. These control experiments clearly show that the methods used to generate spheroplasts were appropriate and retained the integrity of intracellular proteins.

Using spheroplasts prepared from cells expressing T^7 Fat1p, Fat1p^{Q88-HA}, Fat1p^{N579-HA}, and Fat1p^{Y648-HA}, experiments were undertaken using limited proteolysis with trypsin in conjunction with Western blotting to confirm the topological orientation of Fat1p, suggested from the

immunocytochemical studies (Fig. 7). In three cases (T^7 Fat1p, Fat1p^{N579-HA}, and Fat1p^{Y648-HA}), the Fat1p epitope-tagged chimeras within intact spheroplasts were protected from limited proteolysis (using trypsin at up to 1 mg/ml). Fat1p^{Q88-HA}, on the other hand, was less protected from limited proteolysis within intact spheroplasts, consistent with this epitope being exposed on the surface of the membrane. These results are consistent with the immunofluorescence data suggesting that Q⁸⁸ is likely to be on the outer face of the plasma membrane between the two predicted transmembrane helices. When the spheroplasts were permeabilized with Triton X-100, the four epitope-tagged forms of Fat1p had little protection when treated with trypsin (Fig. 7). These data are consistent with a topology of Fat1p in which the amino- and carboxyl-terminal regions are internal and less accessible to limited proteolysis and also are consistent with at least two transmembrane helices in the amino-terminal proximal region of the protein (N_{in} - C_{in} topology). Furthermore, these data are consistent with the conclusion that Fat1p has an externally exposed loop, which is likely to be between residues 37 and 146.

DISCUSSION

This work provides experimental data that defines the topology of the yeast FATP Fat1p. Using spheroplasts prepared from yeast expressing a collection of T^7 - and HA-tagged Fat1p, the immunofluorescence and protease protection data presented in this work are consistent with a N_{in} - C_{in} topological orientation in the plasma membrane. This topology places the ATP/AMP and FATP/VLACS motifs on the interior face of the plasma membrane. The algorithm MEMSTAT3 predicts the third hydrophobic region of Fat1p, which consists of two transmembrane helices separated by a turn consisting of a hydrophobic cap. This topology places the two halves of the ATP/AMP motif (residues 254–271 and 339–356) on the inner face of the membrane. Our previous work has shown that the carboxyl end of Fat1p interacts with the long-chain ACSL Faa1p. The

TABLE 2. Initial rates of lignoceryl-CoA synthetase and fatty acid transport activities of the *fat1Δ faa1Δ* strain transformed with plasmids encoding the different epitope-tagged Fat1p chimeras

Epitope-Tagged Form	4,4-Difluoro-5-methyl-4-bora-3a,4a-diaza- <i>s</i> -indacene-3-dodecanoic Acid Transport	
	$\mu\text{mol}/3 \text{ min}/10^8 \text{ cells}$	$\mu\text{mol}/\text{min}/\text{mg protein}$
T^7 Fat1p	97.9 (8.6)	115.0 (14.6)
Fat1p ^{Q88-HA}	48.2 (6.1)	49.0 (10.4)
Fat1p ^{D193-HA}	ND	ND
Fat1p ^{N579-HA}	57.2 (5.9)	104.1 (20.4)
Fat1p ^{Y648-HA}	34.1 (5.3)	49.3 (6.8)

Values shown in parentheses are SEM ($n = 4$). ND, activity not detectable.

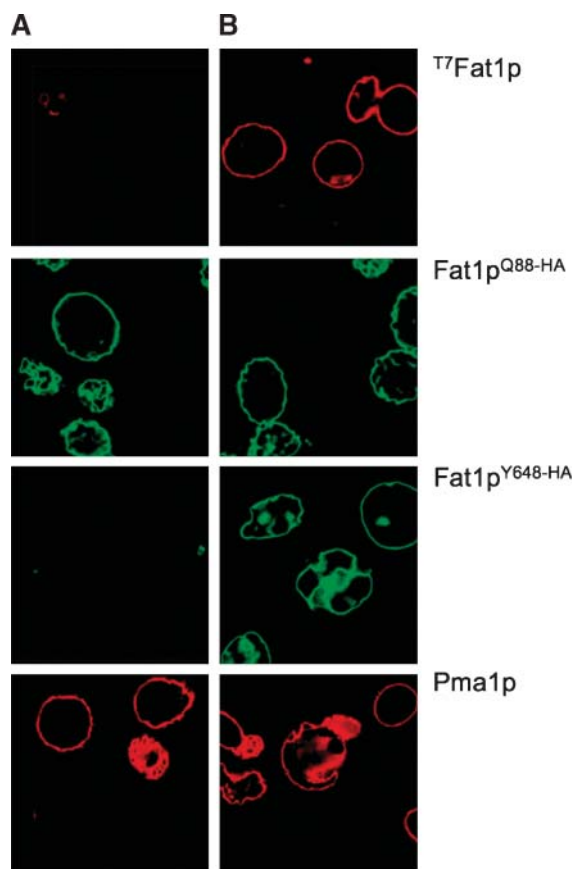


Fig. 5. Immunofluorescence of spheroplasts prepared from cells expressing T^7 Fat1p, Fat1p^{Q88-HA}, and Fat1p^{Y648-HA}. A: Spheroplasted cells fixed and intact. B: Spheroplasted cells fixed and permeabilized. Pma1p was used as a control for plasma membrane with externally exposed regions that are recognized by the polyclonal anti-Pma1p. The images were acquired using a Zeiss SL510 Meta confocal microscope and grouped, and brightness, color balance, and contrast were optimized using Photoshop CS2 (version 9.0; Adobe). The images shown are representative of four independent experiments.

proposed topological orientation of Fat1p places this region on the interior face of the membrane.

The key features of the topology of Fat1p include two transmembrane domains (residues 18–37 and 146–169) that are separated by a loop that is exposed at the membrane surface (Fig. 8). Two additional membrane-associated helices are proposed, the first at residues 278–304 and the second at residues 308–327. These two helices may not traverse the membrane but rather may provide an additional hydrophobic domain, which functions to anchor Fat1p to the membrane. Alternatively, this hydrophobic region may be part of the hydrophobic core of the protein. These two proposed helices are located between the two highly conserved halves of the ATP/AMP motif, which we have shown to be important in both fatty acid transport and very long-chain fatty acid activation. The FATP/VLACS motif that is common to members of the FATP/very long-chain ACSL family is found on the interior face of the membrane and is likely to be in juxtaposition to both elements of the ATP/AMP motif. Finally, the last 110

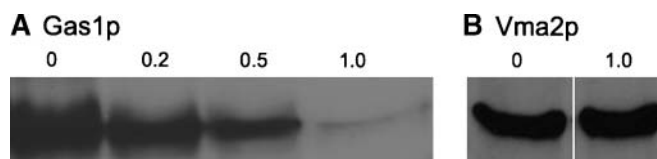


Fig. 6. Western blots showing the integrity of spheroplasts. Spheroplasts were incubated for 30 min with the indicated concentrations of trypsin (mg/ml), and then samples were analyzed using Western blots with anti-Gas1p as an indicator of a plasma membrane-localized protein (A) and anti-Vma2p as an indicator of a intracellular (vacuolar) protein (B). The vertical white line in B indicates splicing of lanes on the same film to generate the composite figure.

amino acid residues of Fat1p are exposed within the cytosol, where they are likely to interact with other proteins. Of particular note, our previous studies identified a dominant negative peptide of Fat1p (residues 545–669) that depresses long-chain ACSL activity associated with the long-chain ACSL Faa1p.

The structures of several adenylate-forming enzymes have been determined, including the ACSL from *Thermus thermophilus*. All three enzymes have similar structures, which we attribute to their adenylate-forming capability. None are membrane-bound or membrane-associated, but nonetheless this structural information offers some insight into the topology of Fat1p. Each contains the highly conserved ATP/AMP, and the two halves of this motif are separated by a helix-rich region that includes three short β -strands. This region of the *T. thermophilus* ACSL contains W²³⁴, which is thought to function as a gating residue for the binding of fatty acids (36). Alignment of this region of Fat1p with *T. thermophilus* ACSL demonstrates considerable divergence, suggesting that these two enzymes are likely to also differ in the structure of this region.

Fat1p has been shown to be an essential component of a complex at the plasma membrane, which also includes an ACSL (either Faa1p or Faa4p) that facilitates the coupled transmembrane movement and activation of exogenous long-chain fatty acids (27). The information generated in this study positions elements of Fat1p, which have been shown to be crucial for protein function, on the interior face of the plasma membrane. Furthermore, previous studies show that a negative dominant peptide of Fat1p (residues 545–669) depresses oleoyl-CoA synthetase activity, which is primarily the result of the ACSL Faa1p. This information, along with yeast two-hybrid studies with the same peptide, supports the conclusion that Faa1p specifically interacts with the carboxyl end of Fat1p. The functional consequence of this interaction is a complex that facilitates the vectorial acylation of exogenous fatty acids. The topological orientation of Fat1p, however, does not provide insights into how this protein functions to traffic exogenous fatty acids across the plasma membrane.

The linkage between Fat1p and a cognate ACSL (either Faa1p or Faa4p) may be structural, in that Fat1p provides a docking platform for ACSL. In this scenario, the activation of fatty acids by either Faa1p or Faa4p represents

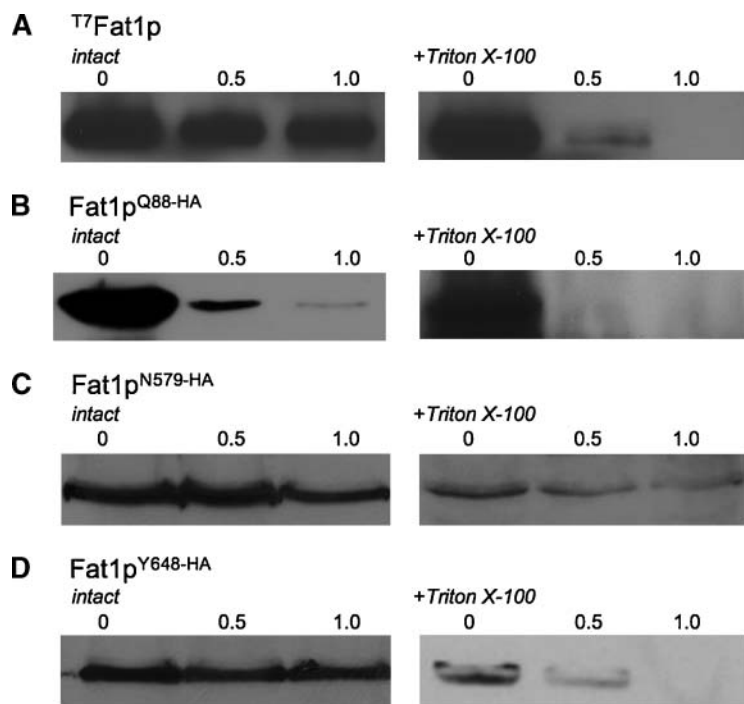


Fig. 7. Western blots after trypsinolysis of intact and permeabilized (+Triton X-100) spheroplasts prepared from cells expressing $T7$ Fat1p (A), Fat1p^{Q88-HA} (B), Fat1p^{N579-HA} (C), and Fat1p^{Y648-HA} (D). The numbers above each lane indicate the concentrations of trypsin used. The blots shown are representative of at least four independent experiments.

the driving force behind the vectorial acylation process. Previous studies from our laboratory fully support this idea. Faergeman et al. (24) showed that yeast strains deficient in both Faa1p and Faa4p fail to accumulate oleoyl-CoA when provided with exogenous oleate. Strains deficient in Fat1p (yet with fully functional Faa1p and Faa4p) were also unable to accumulate oleoyl-CoA when incubated with exogenous oleate (16). The conclusion from this work is that Fat1p facilitates the juxtaposition of ACSL to the plasma membrane, forming a complex that functions to transport exogenous fatty acids concomitant with activation (2). In yeast, this appears to be the primary

mechanism operational in the transport of fatty acids. The topological orientation of Fat1p, and in particular the intracellular localization of the carboxyl region of the protein that interacts with Faa1p and Faa4p, fully supports this fundamental mechanism.

The concept of vectorial acylation as a mechanism driving fatty acid transport was first proposed for Gram-negative bacteria in the late 1960s (44). In this simple system, there is only one ACLS, which is proposed to partition into the bacterial inner membrane, where it functions to abstract fatty acids from the membrane concomitant with activation (45). In mammalian cells, the

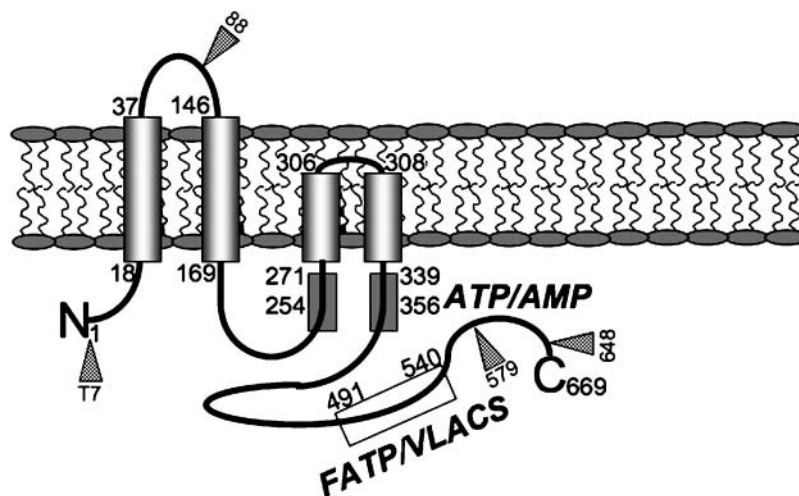



Fig. 8. Topological model of Fat1p. The transmembrane segments are noted as cylinders. The third and fourth hydrophobic regions may simply be membrane-associated regions of Fat1p, as opposed to transmembrane segments. The approximate positions of the ATP/AMP and FATP/very long chain acyl CoA synthetase motifs are noted by the closed and open rectangles, respectively. The locations of the epitope tags in $T7$ Fat1p, Fat1p^{Q88-HA}, Fat1p^{N579-HA}, and Fat1p^{Y648-HA} are noted by the gray arrows, and the numbers indicate amino acid positions along the length of Fat1p.

trafficking of exogenous fatty acids across the plasma membrane is more complex and includes, in addition to FATP and ACSL, FAT/CD36, which has been suggested to deliver free fatty acids to intracellular fatty acid binding proteins (1). Thus, there appear to be two fundamental mechanisms operational in mammalian systems, the first involving FATP and/or ACSL (resulting in vectorial acylation) and the second involving FAT/CD36.

Our laboratory has used the yeast model as a platform to specifically understand the roles of the different FATP and ACSL isoforms in this process (2, 24–27, 46). To date, there are six FATP isoforms defined in mice and humans and five ACSL isoforms defined in mice and rats (47). In addition, there are a number of splice variants, particularly for the ACSL isoforms. This information suggests that the trafficking of fatty acids is rather complex. In yeast, only three of the mice FATP isoforms function in vectorial acylation (mmFATP1, -2, and -4) (23). This argues that each of these proteins must necessarily form a functional linkage with the yeast ACSL. In those cases in which there is no function, the FATP isoforms either have an alternative function, as appears to be the case for mmFATP5, or may not form a functional complex in yeast. What is becoming increasingly apparent is that the concerted activity of the different FATP and ACSL isoforms likely targets fatty acids into defined metabolic pools.

The topological map of Fat1p is quite similar to that of mmFATP1 (48). For mmFATP1, a single transmembrane domain was identified, but in this case as well, the functional elements, including the ATP/AMP and FATP/VLACS motifs, are positioned on the inner face of the plasma membrane. Our previous work has shown that mmFATP1, -2, and -4 are fully functional in the fatty acid import pathway when expressed in yeast (23). The topology of mmFATP1, although similar to that predicted for Fat1p, has a single transmembrane domain, resulting in an $N_{out}-C_{in}$ topology. Lewis et al. (48) showed that the functional elements within mmFATP1 were, like those of Fat1p, located on the interior face of the membrane. Furthermore, these studies with mmFATP1 were consistent with an additional hydrophobic region, which in Fat1p includes residues 275–325 that may function to anchor this protein to the membrane. Studies are under way at present to further define the structure-function relationships within members of the FATP family that are also directed to defining the three-dimensional structures of functional elements within these proteins. 

This work was supported by Grant GM-056840 from the National Institutes of Health. The authors thank Steven Quackenbush and Christopher Petteys for technical assistance.

REFERENCES

- Abumrad, N., C. Coburn, and A. Ibrahim. 1999. Membrane proteins implicated in long-chain fatty acid uptake by mammalian cells: CD36, FATP and FABPm. *Biochim. Biophys. Acta.* **1441**: 4–13.
- Black, P. N., and C. C. DiRusso. 2003. Transmembrane movement of exogenous long-chain fatty acids: proteins, enzymes, and vectorial esterification. *Microbiol. Mol. Biol. Rev.* **67**: 454–472.
- Bonen, A., D. Miskovic, and B. Kiens. 1999. Fatty acid transporters (FABPm, FAT, FATP) in human muscle. *Can. J. Appl. Physiol.* **24**: 515–523.
- Dutta-Roy, A. K. 2000. Cellular uptake of long-chain fatty acids: role of membrane-associated fatty-acid-binding/transport proteins. *Cell. Mol. Life Sci.* **57**: 1360–1372.
- Stahl, A. 2004. A current review of fatty acid transport proteins (SLC27). *Pflugers Arch.* **447**: 722–727.
- Chiu, H. C., A. Kovacs, R. M. Blanton, X. Han, M. Courtois, C. J. Weinheimer, K. A. Yamada, S. Brunet, H. Xu, J. M. Nerbonne, et al. 2005. Transgenic expression of fatty acid transport protein 1 in the heart causes lipotoxic cardiomyopathy. *Circ. Res.* **96**: 225–233.
- Fisher, R. M., and K. Gertow. 2005. Fatty acid transport proteins and insulin resistance. *Curr. Opin. Lipidol.* **16**: 173–178.
- Heron-Milhavet, L., M. Haluzik, S. Yakar, O. Gavrilova, S. Pack, W. C. Jou, A. Ibrahim, H. Kim, D. Hunt, D. Yau, et al. 2004. Muscle-specific overexpression of CD36 reverses the insulin resistance and diabetes of MKR mice. *Endocrinology.* **145**: 4667–4676.
- Herrmann, T., F. van der Hoeven, H. J. Grone, A. F. Stewart, L. Langbein, I. Kaiser, G. Liebisch, I. Gosch, F. Buchkremer, W. Drobnik, et al. 2003. Mice with targeted disruption of the fatty acid transport protein 4 (Fatp 4, Slc27a4) gene show features of lethal restrictive dermopathy. *J. Cell Biol.* **161**: 1105–1115.
- Hubbard, B., H. Doege, S. Punreddy, H. Wu, X. Huang, V. K. Kaushik, R. L. Mozell, J. J. Byrnes, A. Stricker-Krongrad, C. J. Chou, et al. 2006. Mice deleted for fatty acid transport protein 5 have defective bile acid conjugation and are protected from obesity. *Gastroenterology.* **130**: 1259–1269.
- Luiken, J. J., D. P. Koonen, W. A. Coumans, M. M. Pelsers, B. Binas, A. Bonen, and J. F. Glatz. 2003. Long-chain fatty acid uptake by skeletal muscle is impaired in homozygous, but not heterozygous, heart-type-FABP null mice. *Lipids.* **38**: 491–496.
- Moulson, C. L., D. R. Martin, J. J. Lugas, J. E. Schaffer, A. C. Lind, and J. H. Miner. 2003. Cloning of wrinkle-free, a previously uncharacterized mouse mutation, reveals crucial roles for fatty acid transport protein 4 in skin and hair development. *Proc. Natl. Acad. Sci. USA.* **100**: 5274–5279.
- Jia, Z., C. L. Moulson, Z. Pei, J. H. Miner, and P. A. Watkins. 2007. FATP4 is the principal very long-chain fatty acyl-CoA synthetase in skin fibroblasts. *J. Biol. Chem.* **282**: 20573–20583.
- Milger, K., T. Herrmann, C. Becker, D. Gotthardt, J. Zickwolf, R. Ehehalt, P. A. Watkins, W. Stremmel, and J. Fullekrug. 2006. Cellular uptake of fatty acids driven by the ER-localized acyl-CoA synthetase FATP4. *J. Cell Sci.* **119**: 4678–4688.
- Berger, J., C. Truppe, H. Neumann, and S. Forss-Petter. 1998. A novel relative of the very-long-chain acyl-CoA synthetase and fatty acid transporter protein genes with a distinct expression pattern. *Biochem. Biophys. Res. Commun.* **247**: 255–260.
- DiRusso, C. C., E. J. Connell, N. J. Faergeman, J. Knudsen, J. K. Hansen, and P. N. Black. 2000. Murine FATP alleviates growth and biochemical deficiencies of yeast fat1Δ strains. *Eur. J. Biochem.* **267**: 4422–4433.
- Stremmel, W., L. Pohl, A. Ring, and T. Herrmann. 2001. A new concept of cellular uptake and intracellular trafficking of long-chain fatty acids. *Lipids.* **36**: 981–989.
- Watkins, P. A., J. Pevsner, and S. J. Steinberg. 1999. Human very long-chain acyl-CoA synthetase and two human homologs: initial characterization and relationship to fatty acid transport protein. *Prostaglandins Leukot. Essent. Fatty Acids.* **60**: 323–328.
- Hall, A. M., A. J. Smith, and D. A. Bernlohr. 2003. Characterization of the acyl-CoA synthetase activity of purified murine fatty acid transport protein 1. *J. Biol. Chem.* **278**: 43008–43013.
- Hall, A. M., B. M. Wiczler, T. Herrmann, W. Stremmel, and D. A. Bernlohr. 2005. Enzymatic properties of purified murine fatty acid transport protein 4 and analysis of acyl-CoA synthetase activities in tissues from FATP4 null mice. *J. Biol. Chem.* **280**: 11948–11954.
- Black, P. N., N. J. Faergeman, and C. C. DiRusso. 2000. Long-chain acyl-CoA-dependent regulation of gene expression in bacteria, yeast and mammals. *J. Nutr.* **130** (Suppl.): 305–309.
- DiRusso, C. C., and P. N. Black. 1999. Long-chain fatty acid transport in bacteria and yeast. Paradigms for defining the mechanism underlying this protein-mediated process. *Mol. Cell. Biochem.* **192**: 41–52.
- DiRusso, C. C., H. Li, D. Darwis, P. A. Watkins, J. Berger, and P. N. Black. 2005. Comparative biochemical studies of the murine fatty

- acid transport proteins (FATP) expressed in yeast. *J. Biol. Chem.* **280**: 16829–16837.
24. Faergeman, N. J., P. N. Black, X. D. Zhao, J. Knudsen, and C. C. DiRusso. 2001. The acyl-CoA synthetases encoded within FAA1 and FAA4 in *Saccharomyces cerevisiae* function as components of the fatty acid transport system linking import, activation, and intracellular utilization. *J. Biol. Chem.* **276**: 37051–37059.
 25. Faergeman, N. J., C. C. DiRusso, A. Elberger, J. Knudsen, and P. N. Black. 1997. Disruption of the *Saccharomyces cerevisiae* homologue to the murine fatty acid transport protein impairs uptake and growth on long-chain fatty acids. *J. Biol. Chem.* **272**: 8531–8538.
 26. Zou, Z., C. C. DiRusso, V. Ctrnacta, and P. N. Black. 2002. Fatty acid transport in *Saccharomyces cerevisiae*. Directed mutagenesis of FAT1 distinguishes the biochemical activities associated with Fat1p. *J. Biol. Chem.* **277**: 31062–31071.
 27. Zou, Z., F. Tong, N. J. Faergeman, C. Borsting, P. N. Black, and C. C. DiRusso. 2003. Vectorial acylation in *Saccharomyces cerevisiae*. Fat1p and fatty acyl-CoA synthetase are interacting components of a fatty acid import complex. *J. Biol. Chem.* **278**: 16414–16422.
 28. Richards, M. R., J. D. Harp, D. S. Ory, and J. E. Schaffer. 2006. Fatty acid transport protein 1 and long-chain acyl coenzyme A synthetase 1 interact in adipocytes. *J. Lipid Res.* **47**: 665–672.
 29. Gietz, R. D., R. H. Schiestl, A. R. Willems, and R. A. Woods. 1995. Studies on the transformation of intact yeast cells by the LiAc/SS-DNA/PEG procedure. *Yeast*. **11**: 355–360.
 30. Kyte, J., and R. F. Doolittle. 1982. A simple method for displaying the hydropathic character of a protein. *J. Mol. Biol.* **157**: 105–132.
 31. Hofmann, K., and W. Stoffel. 1993. TMbase—a database of membrane spanning protein segments. *Biol. Chem. Hoppe Seyler*. **374**: 166.
 32. McGuffin, L. J., K. Bryson, and D. T. Jones. 2000. The PSIPRED protein structure prediction server. *Bioinformatics*. **16**: 404–405.
 33. Schwede, T., J. Kopp, N. Guex, and M. C. Peitsch. 2003. SWISS-MODEL: an automated protein homology-modeling server. *Nucleic Acids Res.* **31**: 3381–3385.
 34. Conti, E., N. P. Franks, and P. Brick. 1996. Crystal structure of firefly luciferase throws light on a superfamily of adenylate-forming enzymes. *Structure*. **4**: 287–298.
 35. Jogl, G., and L. Tong. 2004. Crystal structure of yeast acetyl-coenzyme A synthetase in complex with AMP. *Biochemistry*. **43**: 1425–1431.
 36. Hisanaga, Y., H. Ago, N. Nakagawa, K. Hamada, K. Ida, M. Yamamoto, T. Hori, Y. Arai, M. Sugahara, S. Kuramitsu, et al. 2004. Structural basis of the substrate-specific two-step catalysis of long chain fatty acyl-CoA synthetase dimer. *J. Biol. Chem.* **279**: 31717–31726.
 37. Zinser, E., and G. Daum. 1995. Isolation and biochemical characterization of organelles from the yeast, *Saccharomyces cerevisiae*. *Yeast*. **11**: 493–536.
 38. Li, H., P. N. Black, and C. C. DiRusso. 2005. A live-cell high-throughput screening assay for identification of fatty acid uptake inhibitors. *Anal. Biochem.* **336**: 11–19.
 39. Garnier, C., M. O. Blondel, and R. Haguenaer-Tsapis. 1996. Membrane topology of the yeast uracil permease. *Mol. Microbiol.* **21**: 1061–1073.
 40. Gertow, K., C. Skoglund-Andersson, P. Eriksson, S. Boquist, K. Orth-Gomer, K. Schenck-Gustafsson, A. Hamsten, and R. M. Fisher. 2003. A common polymorphism in the fatty acid transport protein-1 gene associated with elevated post-prandial lipaemia and alterations in LDL particle size distribution. *Atherosclerosis*. **167**: 265–273.
 41. Kelley, L. A., R. M. MacCallum, and M. J. Sternberg. 2000. Enhanced genome annotation using structural profiles in the program 3D-PSSM. *J. Mol. Biol.* **299**: 499–520.
 42. Black, P. N., C. C. DiRusso, D. Sherin, R. MacColl, J. Knudsen, and J. D. Weimar. 2000. Affinity labeling fatty acyl-CoA synthetase with 9-p-azidophenoxy nonanoic acid and the identification of the fatty acid-binding site. *J. Biol. Chem.* **275**: 38547–38553.
 43. Athenstaedt, K., D. Zweyck, A. Jandrositz, S. D. Kohlwein, and G. Daum. 1999. Identification and characterization of major lipid proteins of the yeast *Saccharomyces cerevisiae*. *J. Bacteriol.* **181**: 6441–6448.
 44. Overath, P., G. Pauli, and H. U. Schairer. 1969. Fatty acid degradation in *Escherichia coli*. An inducible acyl-CoA synthetase, the mapping of old-mutations, and the isolation of regulatory mutants. *Eur. J. Biochem.* **7**: 559–574.
 45. DiRusso, C. C., and P. N. Black. 2004. Bacterial long chain fatty acid transport: gateway to a fatty acid-responsive signaling system. *J. Biol. Chem.* **279**: 49563–49566.
 46. Black, P. N., and C. C. DiRusso. 2007. Yeast acyl-CoA synthetases at the crossroads of fatty acid metabolism and regulation. *Biochim. Biophys. Acta*. **1771**: 286–298.
 47. Doege, H., and A. Stahl. 2006. Protein-mediated fatty acid uptake: novel insights from in vivo models. *Physiology (Bethesda)*. **21**: 259–268.
 48. Lewis, S. E., L. L. Listenberger, D. S. Ory, and J. E. Schaffer. 2001. Membrane topology of the murine fatty acid transport protein 1. *J. Biol. Chem.* **276**: 37042–37050.